Exploring Intramolecular Reactions in Complex Systems with Metadynamics: The Case of the Malonate Anions

Eliana Asciutto and Celeste Sagui*

Center for High Performance Simulations and Department of Physics, North Carolina State University, Raleigh, North Carolina 27695-8202

Received: June 23, 2005

We have determined the optimized structures, relative energies and intramolecular reactions for two anionic forms of malonic acid, anion malonate(−1) ($HO_2CCH_2CO_2^-$) and malonate(−2) ($^-O_2CCH_2CO_2^-$). For this purpose we employed accurate quantum chemistry calculations using second-order Möller−Plesset perturbation theory and Density Functional Theory with an aug′-cc-p-VTZ basis set to determine the structures and energies, and a novel metadynamics method based on Car−Parrinello molecular dynamics for the thermal reactions. For both malonates, we found new isomers (keto and enol structures) characterized by CO_2 rotations and intramolecular proton transfers. These proton transfers characterize the keto−enol tautomerism that takes place both in the monoanion and dianion. In all cases, the keto tautomer is the more stable configuration. The metadynamics method allows the system to explore the potential energy surface in a few picoseconds, crossing activation barriers of 20−50 kcal/mol.

I. Introduction

Malonic acid belongs to the important family of carboxylic acids. There have been numerous computational studies on carboxylic acids—in particular the simplest ones, namely formic and acetic acids.[1−7] The motivation for the studies of these acids and their anions is to gain an understanding of the chemistry of the acid moiety itself, proton transfer,[4,5,8,9] the geometry of excited states,[2,9] and the existence of multiple charged anions in the gas and solvated phases.[10−14] In terms of its technological significance, synthetic compounds based on malonic acid can act as inhibitors of matrix metalloproteinases that cause tissue remodeling and related diseases, such as tumor invasion and joint destruction.[15] Malonates have also been used as a model for γ-carboxyglutamic acid (formed by a posttranslational, Vitamin K-mediated carboxylation of specific glutamyl residues).[16] In addition, malonic acid and its corresponding anions are among the most abundant dicarboxylates found in natural water. They are particularly important compounds in the formation waters of oil fields in the crust of the earth, where the speciation of malonates depends on the pH.[17]

Understanding the different conformations of malonic acid ($HO_2CCH_2CO_2H$) and its anions malonate(−1) ($HO_2CCH_2CO_2^-$) and malonate(−2) ($^-O_2CCH_2CO_2^-$) has proved to be a challenging problem for both theorists and experimentalists.[8,9,17−22] While there have been some quantum chemistry investigations of the different isomers, a complete identification of the global minima and transition states (TS) has so far proved elusive. Recently, Deerfield and Pedersen[20] measured the relative energies of the anions with respect to the acid, as well as the difference between the keto and enol tautomers of the monoanion and of the dianion. They also studied the influence of metal ion coordination on the acidity. Maçôas et al.[21] studied the relative energies and vibrational spectra of the conformational states of the malonic acid monomer, using various levels of approximations. Their calculations predict the existence of six different conformers, three of which were found with low energies close enough to enable their spectroscopic observation. Their more accurate calculations agreed well with their analysis of the infrared spectra of monomeric malonic acid isolated in a solid argon matrix. Herbert and Ortiz[22] used the Moller−Plesset to second order (MP2) method with the 6-31+G* and the 6-31++G(d,p) basis sets to identify some of the isomers of the dianion $^-O_2CCH_2CO_2^-$ as well as the monoanion $O_2CCH_2CO_2^-$ obtained by eliminating one electron of the dianion. Unfortunately, in some cases the basis set 6-31++G(d,p) is not accurate enough for the proper identification of global minima and/or transition states.

In this work, we have set out to identify the different minima and transition states of the malonate anions by exploring the free energy surface (FES) with a recently introduced method named metadynamics.[23,24] An elucidation of the long-lived metastable configurations and the transition states is often crucial for the understanding of the chemical and biological functions of a molecule. However for most molecules, the theoretical investigation of these important states is notoriously difficult. The FES of most molecules is quite complex, with large free energy barriers separating the different configurations. Very long time scales are needed in order to fully explore a given FES, which is generally precluded in a regular molecular dynamics simulation. The metadynamics method is based on the ideas of extended Lagrangian and coarse-grained non-Markovian dynamics ([25−27]), and it allows for different pathways to explore rare events in systems with complex potential energy surfaces. Although there is a great number of techniques to describe complex chemical reactions, these techniques tend to fail when the FES is very complex or when the entropic contribution cannot be neglected. The metadynamics method can explore complex reaction paths involving several energy barriers in a very short time. Even when the exact transition state geometry may not be achieved during a metadynamics simulation, the trajectory generally samples states that are very close. It can, therefore, be used to obtain an initial guess for more standard optimization techniques that can thus easily optimize geometries for both the transition states and previously unknown minima. The use of this method, together with highly accurate quantum

10.1021/jp053428z CCC: $30.25
Published on Web 08/06/2005

calculations, has allowed us to achieve a new characterization of the relative and absolute minima, as well as the transition states of the malonate anions.

II. Computational Methodology

A. The Metadynamics Method. The metadynamics method allows for a quick and efficient sampling of the configurational space. This is usually difficult to achieve with a regular MD simulation if the TS barriers are relatively high. Details of the metadynamics method have previously been published[23,24] and will only be briefly reviewed here. The first crucial step in the method is to identify the *collective variables* (CV), $S_a(\mathbf{R})$, $a = 1, ..., n$, which are analytic functions of the ionic positions $\mathbf{R}$. The CVs must include all the relevant modes that cannot be sampled in the time scale of the simulation, as well as be able to distinguish between reactants and products. Typical CVs include distances between atoms, dihedral or torsional angles, coordination numbers, etc. The metadynamics trajectory is defined within the context of the Car−Parrinello Lagrangian[25] by introducing an extended, time-dependent Lagrangian:

$$L = L_{\mathrm{CP}} + \sum_a \frac{1}{2} M_a \dot{s}_a^{\,2} - \sum_a \frac{1}{2} k_a (S_a(\boldsymbol{R}) - s_a)^2 - V(t,\{s_a\}) \tag{2.1}$$

where L_{CP} is the standard Car−Parrinello Lagrangian that drives the electronic and ionic dynamics. Each selected $S_a(\mathbf{R})$ is coupled to an additional dynamic variable s_a through a harmonic potential $1/2k_a(S_a(\mathbf{R}) - s_a)^2$. The second term in the Hamiltonian is the fictitious kinetic energy of the $\{s_a\}$ and $V(t,\{s_a\})$ is a time-dependent potential constructed as a sum of repulsive, hill-like potentials that prevent the system from visiting previously explored configurations. The history-dependent potential fills the free energy wells and drives the system from one minimum to the other crossing saddle points. $V(t,\{s_a\})$ is constructed by superimposing a series of Gaussians. For the vectors $\boldsymbol{s} = \{s_a\}$ and $\mathbf{s}^i = \{s_a(t_i)\}$, $V(t, \mathbf{s})$ has the following form:

$$V(t, \mathbf{s}) = \sum_{t_i < t} W_i \exp\left[-\frac{(\mathbf{s} - \mathbf{s}^i)^2}{2(\Delta s^{\perp})^2}\right] \exp\left[-\frac{[(\mathbf{s}^{i+1} - \mathbf{s}^i)\cdot(\mathbf{s} - \mathbf{s}^i)]^2}{2(\Delta s^{\parallel}{}_i)^4}\right] \tag{2.2}$$

The shape of the Gaussian is adapted to the topology of the energy surface. In particular, $\Delta s^{\perp}$ gives the size of the Gaussians in a direction perpendicular to the motion while $\Delta s^{\parallel}{}_i = |\mathbf{s}^{i+1} - \mathbf{s}^i|$ gives the size along the direction of motion. W_i is an adaptive prefactor calculated from the average of the harmonic force involving the CVs, to counterbalance the force coming from the original FES. The mass M_a and the coupling constant k_a determine how fast s_a evolves with respect to the ionic and electronic degrees of freedom. If the values of M_a and k_a are chosen so that the dynamics of $\{s_a\}$ is adiabatically decoupled from the faster ionic and electronic motion, then $V(t, \mathbf{s})$ approaches the free energy of the system $F(\mathbf{s})$:

$$V(t, \mathbf{s})_{t\to\infty} = -F(\mathbf{s}) \tag{2.3}$$

within a constant. The accuracy of the evaluation of the free energy profile depends on the size of the time-dependent potential's hills. For low accumulation rates,[23,24] the accuracy in the resolution of the free energy is a few kilocalories per mole.

Metadynamics simulations were carried out using the CPMD code,[28] with the LYP correlation energy[29] and the OPTX exchange energy functional.[30] The electronic description used Vanderbilt pseudopotentials[31] with a 45 Ry energy cutoff. Metadynamics molecular dynamics (MD) simulations driven by the Lagrangian in (2.1) were carried out at $T = 300$ K. They used a time step of 0.12 fs, a fictitious electron mass of 800 a.u, and $V(t, \mathbf{s})$ was updated every 0.001 ps.

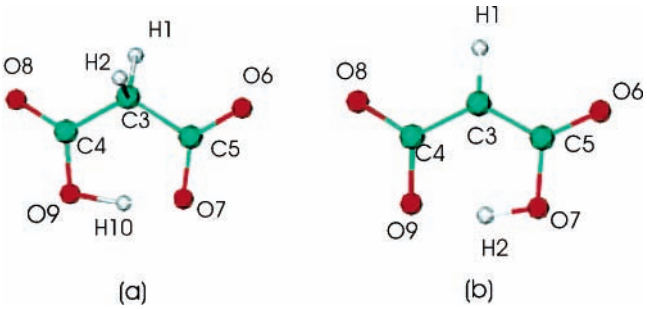

Figure 1. Atomic labeling for (a) malonate monoanion, and (b) malonate dianion. In this convention, we label H10 in the monoanion as the proton always bonded to O9 (it can also jump to O7), H1 is always bonded to C3, while H2 can be bonded either to C3 (keto) or O7 (enol), determining the nature of the tautomer. In the dianion, H1 is always bonded to C3, and H2 to either C3 (keto) or O7 (enol) in the equilibrium states, or to O8 in the transition state keto 1 → enol 1 (Figure 3d). Naturally, in the enol forms H2 can jump between the symmetric positions at O7 and O9.

B. Accurate Quantum Chemistry Calculations. Minima and transition states of the malonate anions were determined with four different calculations. First, we used the MP2 method as implemented in the Gaussian 03[32] program, for the energy calculations in gas phase. Since a correct description of these potential energy hypersurfaces requires large basis sets in conjunction with a high-level treatment of electron correlation effects, an aug′-cc-p-VTZ basis set (Dunning's polarized valence triple-split basis set augmented with diffuse functions on nonhydrogen atoms[33]) was used. (smaller basis set like 6-31++G-(d,p) failed to properly determine some of the minima and/or TS). Second, we performed all-electron density functional theory (DFT) calculations in gas phase, using the same basis set and the BLYP[29,34] functional, as provided by Gaussian 03. Third, we repeated this last calculation with a continuous solvent model based on the Onsager model,[35] where the solute is placed in a spherical cavity immersed in a continuous medium having the dielectric constant of water. (Unfortunately we were not able to determine the TS enol 1 → enol 2 in this approximation). Fourth, we carried out exact geometry calculations using the CPMD code,[28] with the LYP correlation energy and the OPTX exchange energy functional.[30] The electronic description used Vanderbilt pseudopotentials[31] with a 45 Ry energy cutoff. These calculations compared very well with the results obtained from both MP2 and DFT with the aug′-cc-p-VTZ basis set, which validates the metadynamics results. In all cases, a normal-mode analysis was performed to confirm the nature of the stationary points.

III. Structural Results

Atomic labels for the monoanion and dianion are given in Figure 1, parts a and b, respectively. Here, label H10 in the monoanion represents the proton that is always bonded to O9 (it can also jump to O7); H1 is always bonded to C3; and H2 can be bonded either to C3 (keto) or O7 (enol), thereby determining the nature of the tautomer. In the dianion, H1 is always bonded to C3, and H2 is bonded to either C3 (keto) or O7 (enol) in the equilibrium states or to O8 in the transition state keto 1 → enol 1. Results for the relative energies are presented in Table

TABLE 1: Relative Energies of the Deprotonated Forms of Malonic Acid[a]

	MP2	BLYP	solvent
monoanion			
keto 1	0.0	0.0	0.0
keto 2	19.3	16.8	11.3
enol 1	20.3	17.7	14.4
enol 2	25.5	22.4	20.1
TS keto 1 → keto 2	23.1	20.1	11.4
TS enol 1 → enol 2	33.4	29.6	
dianion			
keto 1	0.0	0.0	0.0
enol 1	7.2	8.0	8.4
enol 2	28.7	27.3	25.3
TS keto 1 → enol 1	49.7	47.9	26.4
TS enol 1 → enol 2	34.9	32.5	

[a] The relative energies are given in kilocalories per mole and include zero point energy corrections. Both the MP2 and DFT-BLYP calculations use the aug′-cc-p-VTZ basis set. The energies in the "solvent" column are computed using the DFT-BLYP approximation with the continuum dielectric Onsager model. TS stands for transition state.

1 and for the structural parameters in Tables 2−4. For comparison purposes, results obtained using the BLYP density energy functional with the same basis set are shown in Table 1, and structural results for the OLYP exchange energy functional (obtained with the CPMD code) are presented in Tables 2−4. We found that the DFT/OLYP calculations with Vanderbilt pseudopotentials gave better values than the all-electron DFT BLYP/aug′-cc-p-VTZ description (measured with respect to the MP2 calculations). For the bonds and dihedrals angles, these values are less than 1% higher than the ones obtained with the more accurate MP2/aug′-cc-p-VTZ calculation; for the torsional angles the agreement is somewhat less good.

A. Malonate Monoanion. Optimization of the monoanion (hydrogen malonate) geometries gave the structures shown in Figure 2. In all the structures, one of the acid groups always contains 1 hydrogen atom (−COOH), while the other group may bear the negative charge (*keto* tautomer), or may also be attached to a hydrogen (*enol* tautomer), in which case the middle C bears the negative charge. Four minima were found, with the two keto forms are lower in energy than the two enol forms. The global minimum is a planar carbon−oxygen ring configuration (Figure 2a), with the proton H10 lying in the inner part of the carbon ring. The proton is slightly closer to one of the two oxygens, and during metadynamics simulations it frequently jumps between the oxygens. In fact, the configuration where H10 is exactly equidistant from O7 and O9 (not shown) represents a transition state with a tiny energy barrier of ∼0.18 kcal/mol.

Conformation b is characterized by a rotation of the CO_2 moiety; this is the most polar structure (with a dipolar moment $\mu = 6.7$ D), and therefore the structure is stabilized considerably when solvent effects are included. The transition states between the keto minima (a and b) are shown in Figure 2c. The first planar enol form shown in part d is just 1 kcal/mol higher than the very different keto 2 structure. The second planar form shown in part e is a totally symmetric configuration. The transition states between the enol minima (d and e) are shown in Figure 2f. Out of the six stationary states presented here, only part e has been reported previously.[20]

B. Malonate Dianion. Optimization of the malonate dianion geometries resulted in the structures shown in Figure 3. The global minimum corresponds to a keto structure (Figure 3a), with the two CO_2 groups laying on perpendicular planes. The C−C bond lengths are longer than in the other conformations, while the dihedral C−C−C angle is the smallest one. The other internal angles are completely symmetrical. In addition, we found two enol structures. The relative energy of the enol 1

TABLE 2: Optimized Bond Lengths (Å) at the MP2 Level[a]

	C4−C3	C3−C5	C4−O8	C4−O9	C3−H1	C5−O6	C5−O7
monoanion							
keto 1	1.53(1.54)	1.54(1.55)	1.23(1.24)	1.31(1.32)	1.09(1.10)	1.23(1.25)	1.29(1.31)
keto 2	1.48(1.48)	1.59(1.64)	1.22(1.23)	1.37(1.39)	1.09(1.10)	1.25(1.26)	1.25(1.25)
enol 1	1.43(1.44)	1.40(1.41)	1.23(1.24)	1.38(1.40)	1.08(1.09)	1.24(1.25)	1.43(1.44)
enol 2	1.41(1.42)	1.41(1.42)	1.24(1.25)	1.39(1.41)	1.08(1.09)	1.24(1.25)	1.39(1.41)
TS k1-k2	1.48(1.48)	1.60(1.64)	1.21(1.22)	1.40(1.41)	1.09(1.10)	1.24(1.25)	1.25(1.26)
TS e1-e2	1.41(1.42)	1.41(1.42)	1.23(1.24)	1.42(1.44)	1.08(1.09)	1.24(1.25)	1.39(1.41)
dianion							
keto 1	1.56(1.57)	1.56(1.57)	1.27(1.28)	1.26(1.27)	1.09(1.10)	1.27(1.28)	1.26(1.27)
enol 1	1.46(1.46)	1.41(1.43)	1.27(1.29)	1.31(1.33)	1.08(1.09)	1.26(1.27)	1.38(1.39)
enol 2	1.50(1.50)	1.38(1.39)	1.28(1.30)	1.27(1.28)	1.08(1.09)	1.28(1.29)	1.43(1.44)
TS k1-e2	1.50(1.51)	1.51(1.51)	1.37(1.38)	1.23(1.24)	1.09(1.10)	1.28(1.29)	1.27(1.28)
TS e1-e2	1.51(1.51)	1.38(1.39)	1.28(1.30)	1.27(1.28)	1.09(1.10)	1.26(1.28)	1.45(1.47)

[a] Values calculated with DFT with the OLYP functional and Vanderbilt pseudopotentials as implemented in the CPMD code are given in parentheses.

TABLE 3: Optimized Dihedral Angles (deg) at the MP2 Level[a]

	C4−C3−C5	C3−C4−O9	C3−C5−O7	O8−C4−O9	O6−C5−O7	H1−C3−C4	H1−C3−C5
monoanion							
keto 1	118(118)	115(115)	115(115)	125(124)	126(126)	109(107)	109(107)
keto 2	111(114)	112(113)	116(117)	120(120)	132(132)	111(111)	107(106)
enol 1	130(131)	118(119)	115(115)	117(116)	115(115)	115(115)	115(115)
enol 2	131(133)	117(118)	117(118)	116(116)	117(116)	115(114)	115(114)
TS k1-k2	107(111)	112(112)	115(116)	121(120)	131(131)	111(111)	107(105)
TS e1-e2	131(133)	116(117)	118(118)	118(117)	116(116)	115(114)	114(113)
dianion							
keto 1	119(120)	116(117)	116(117)	127(126)	127(127)	107(107)	107(108)
enol 1	125(125)	117(117)	115(115)	122(122)	118(118)	118(118)	117(117)
enol 2	133(134)	121(121)	119(119)	125(124)	112(112)	115(114)	112(112)
TS k1-e2	125(127)	135(135)	118(119)	122(122)	125(125)	108(109)	111(112)
TS e1-e2	133(134)	121(121)	116(117)	125(124)	115(114)	114(113)	113(112)

[a] Values calculated with DFT with the OLYP functional and Vanderbilt pseudopotentials as implemented in the CPMD code are given in brackets.

TABLE 4: Optimized Torsional Angles (deg) at the MP2 Level[a]

	C3−O8−C4−O9	C3−O6−C5−O7	O8−C4−C3−H1	O6−C5−C3−H1
monoanion				
keto 1	179(179)	179(179)	47(78)	47(79)
keto 2	179(178)	180(180)	146(148)	58(55)
enol 1	180(180)	180(180)	0.004(0.14)	0.02(0.15)
enol 2	180(180)	180(180)	0.04(0.05)	0.03(0.10)
TS k1-k2	176(176)	180(180)	143(141)	65(63)
TS e1-e2	177(177)	178(178)	4.04(4.29)	4.34(4.43)
dianion				
keto 1	176(176)	176(176)	114(114)	1.97(3.27)
enol 1	180(180)	180(180)	0.15(0.49)	0.09(0.06)
enol 2	180(180)	180(180)	0.04(0.23)	0.01(0.04)
TS k1-e2	180(180)	177(176)	81(81)	20(17)
TS e1-e2	178(178)	178(178)	12(12)	5(6)

[a] Values calculated with DFT with the OLYP functional and Vanderbilt pseudopotentials as implemented in the CPMD code are given in brackets.

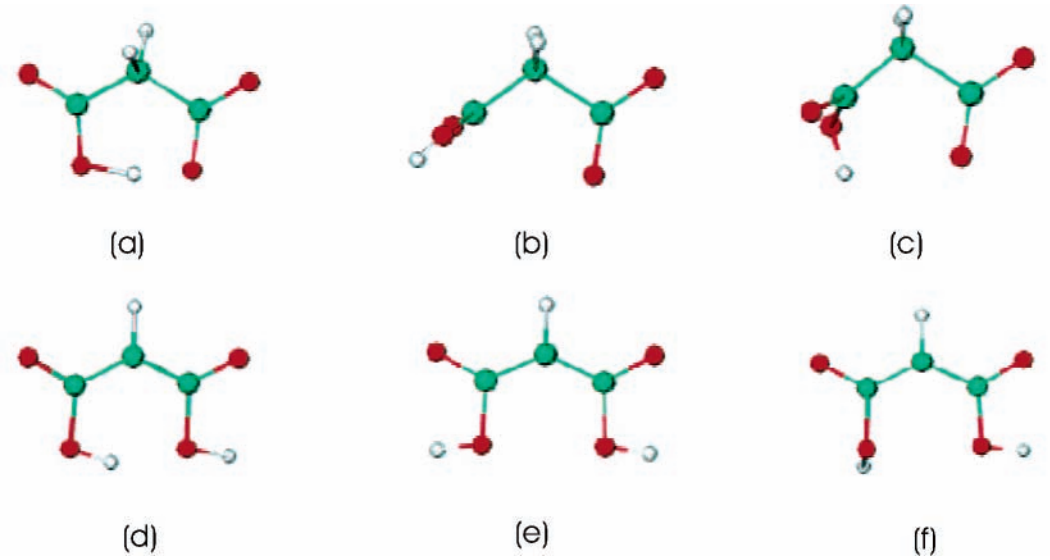

Figure 2. Optimized structures for the malonate anion. Relative energies are given in Table 1. (a) keto 1 configuration; (b) keto 2 configuration; (c) TS between (a) and (b); (d) enol 1 configuration; (e) enol 2 configuration; (f) TS between (d) and (e).

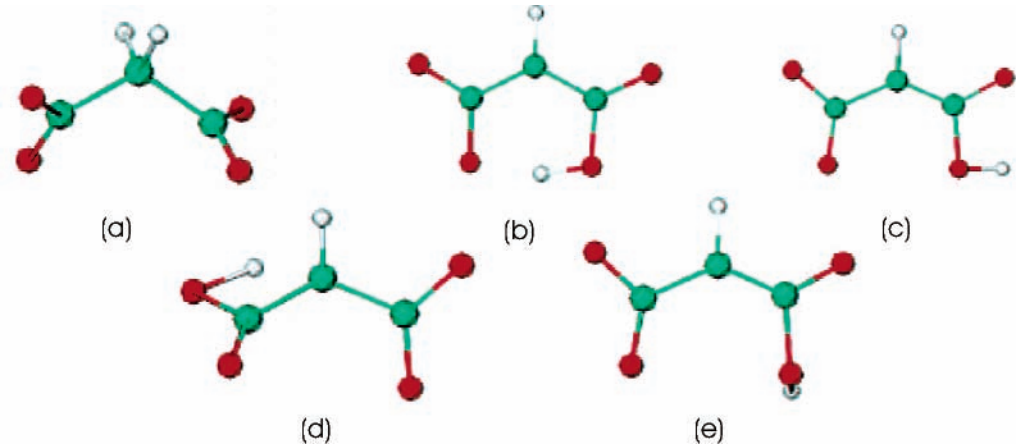

Figure 3. Optimized structures for the malonate dianion. Relative energies are given in Table 1. Key: (a) keto 1 configuration; (b) enol 1 configuration; (c) enol 2 configuration; (d) TS between parts a and b; (e) TS between parts b and c.

configuration (Figure 3b) with respect to the keto 1 tautomer is measured as 7.2 kcal/mol (MP2/aug′-cc-p-VTZ). This is the least polar structure ($\mu = 1.7$ D), and therefore, there is almost no difference in energy when solvent effects are included. The other enol form, identified as the enol 2 structure (Figure 3c), has a relative energy of 28.7 kcal/mol (MP2/aug′-cc-p-VTZ). The geometry not only differs from the other enol form in the position of the H2 atom, but it also has bigger internal angles and the carbon ring is wider.

We were able to identify two transition states. The TS keto 1 → enol 1 (Figure 3d), has a very large energy barrier of 49.7 kcal/mol in gas phase (MP2/aug′-cc-p-VTZ). When solvent effects are considered, this barrier is reduced to 26.4 kcal/mol. The TS enol 1 → enol 2 (Figure 3e) has a structure with an energy of 34.9 kcal/mol in the gas phase (MP2/aug′-cc-p-VTZ) relative to the global minimum. To the best of our knowledge, these transition states have not been identified before.

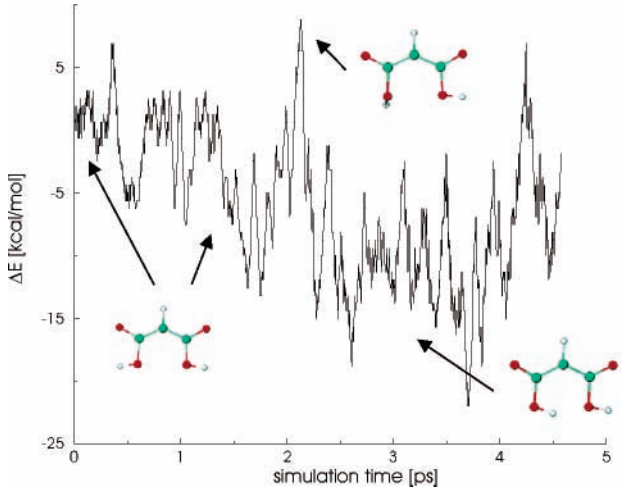

Figure 4. Potential energy evolution as obtained from metadynamics during the enol 2 → enol 1 monoanion reaction. $\Delta s^{\perp} = 0.1$; $W_i = 0.6$ kcal/mol; $M_a = 40$ amu; $k_a = 0.2$ amu.

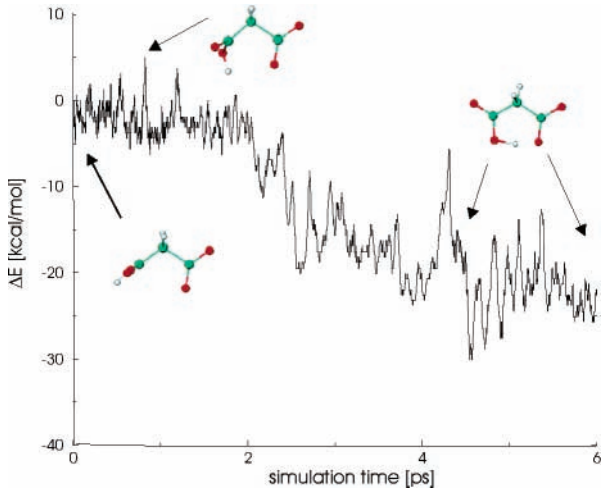

Figure 5. Potential energy evolution as obtained from metadynamics during the keto 2 → keto 1 monoanion reaction. $\Delta s^{\perp} = 0.1$; $W_i = 0.6$ kcal/mol; $M_a = 40$ amu; $k_a = 0.2$ amu.

Finally, the absolute minimum of the dianion is higher than that of the monoanion: −415.674774 vs −416.405711 au. The malonate dianion has not been seen experimentally in gas phase,[22] although one to three molecules of waters seem enough to stabilize it in electrospray experiments.[36] Yet, we believe that a complete understanding of the dianion in water requires first a clear knowledge of the intramolecular potentials. In this sense, our work is similar to other published work, where studies of the intramolecular potentials are carried out.[20,37,38]

IV. Metadynamics Results

Here we discuss salient features of the metadynamics runs, that helped in the elucidation of some of the minima/TS as well as revealed the mechanisms in conformational changes or intramolecular proton transfer. In this work, we present curves of the energy vs the simulation time. In many cases, the minima and maxima of the curves are easy to visualize; in a few cases the noise in the energy may make it a little less obvious. Fortunately, in those "doubtful" cases, one has other variables, such as the collective variables as a function of time and—most practical—dynamics of the reaction that can be visualized through movies, that help discern between the different states.

A. Malonate Monoanion. We performed two metadynamics runs where the time dependent potential was constructed using small Gaussians (whose height was about 1% of the barriers involved). The width of the Gaussians was chosen as $\Delta s^{\perp} = 0.1$ and the height was chosen as $W_i = 0.6$ kcal/mol. In the first run (Figure 4), we started from the enol 2 conformation (Figure 2e), and chose as CVs the H10−O8 distance and the H10−C3−H1 angles. At the beginning of the simulation, the H10 proton moves rapidly around its equilibrium position. Within only 2.5 ps the well is filled and the proton can finally rotate reaching the TS. After crossing this barrier the molecule goes directly to the enol 1 structure. The free energy barrier calculated using the approximation (2.3) is ∼10 kcal/mol. (In the MP2 calculation, this is 7.9 kcal/mol, see Table 1).

A second metadynamic run starting from the keto 2 tautomer was performed. The reaction coordinates chosen in this case were the H10−O7 distance,the torsional angle C3−C4−O8−O9 and the dihedral angle C4−O9−H10. As can be seen in Figure 5, the TS between these keto structures is reached in ≈1 ps. After that, we observed several rotations of the C4−O8−O9−H10 moiety, until the system finally crosses the 5 kcal/mol barrier and further lowers its energy by rotating both

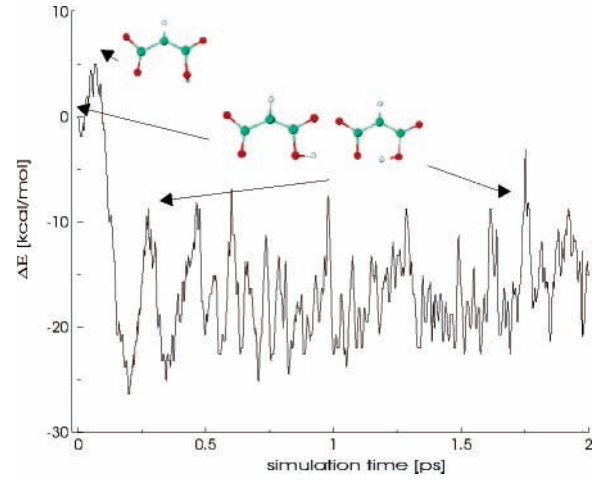

Figure 6. Potential energy evolution as obtained from metadynamics during the enol 2 → enol 1 dianion reaction. $\Delta s^{\perp} = 0.05$; $W_i = 0.3$ kcal/mol; $M_a = 40$ amu; $k_a = 1.5$ amu.

O−C−O moieties. Finally, after 4 ps of simulation, the system falls into the global minimum—the keto 1 structure—lying ≈20 kcal/mol below the initial configuration. The free energy barrier calculated from the metadynamics approximation (2.3) is estimated to be about 4 kcal/mol, which compares reasonably well with the 3.3 kcal/mol result based on the MP2 calculation.

B. Malonate Dianion. The first simulation, presented in Figure 6, started from the enol 2 configuration in Figure 3c. To study the reaction from this configuration to the enol 1 tautomer (Figure 3b), we found that the best choice for the CVs is the dihedral angle C3−C5−H2 and the torsional angle O8−C4−C3−C5. Although this reaction involves a similar rearrangement to the corresponding reaction studied for the anion malonate, the energy well is filled almost inmediately after the simulation starts (Figure 6). The H2 atom reaches the TS with an energy barrier ≈7kcal/mol and then, in just 0.25 ps, forms the enol 1 configuration. For the rest of the simulation, the proton keeps jumping between O9 and O7.

Figure 7 shows details of a second metadynamics run, which shows the mechanisms of intramolecular proton transfer. Starting from the enol 1 structure (Figure 3b) we were able to observe the transition to the global minimum, keto 1 tautomer (Figure 3a). The reaction coordinates were chosen to be the same as in the previous reaction: the C3−C5−H2 dihedral angle and the

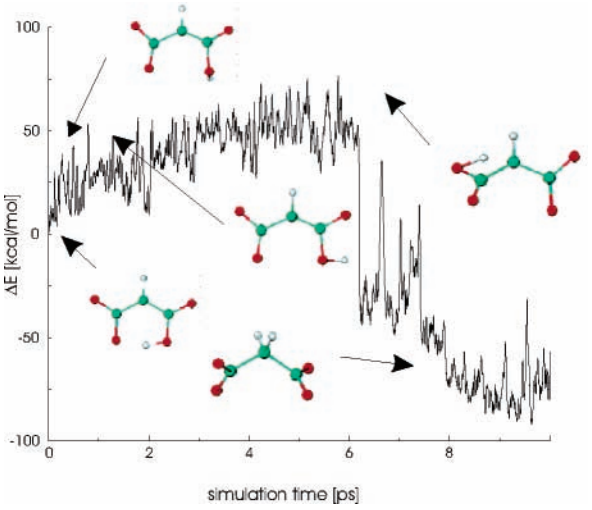

Figure 7. Potential energy evolution as obtained from metadynamics during the enol 1 → keto 1 dianion reaction. $\Delta s^{\perp} = 0.2$; $W_i = 5-15$ kcal/mol.

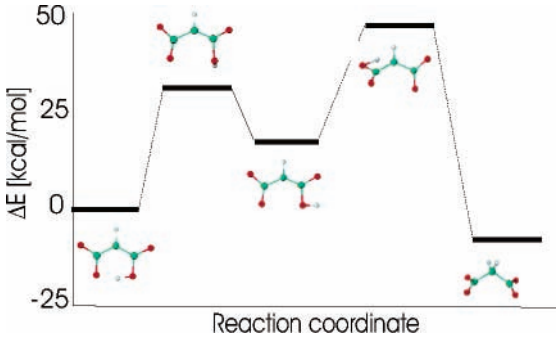

Figure 8. Reaction energy profile as obtained from metadynamics for the enol 1 → keto 1 reaction.

O8−C5−C3−C4 torsional angle. However, we had to use a limiting case with larger Gaussians (width = 0.2 and height ≈6 kcal/mol) and smaller masses (1 amu), (in this case, the approximation in (2.3) is no longer valid). First, we observed the H2 proton jumping between the two oxygens (O7 and O9) in the enol 1 configuration, crossing several times the tiny barrier. It takes approximately 1 ps for the H2 to cross the first barrier (TS enol 1 → enol 2), making a rotation in order to reach the higher-energy enol 2 configuration. Then the system jumps several times between these two states (enol 2 and enol 1), crossing intermediate states characterized by torsional rotations driven by the O8−C5−C3−C4 reaction coordinate and the proton transfer between the two adjacent oxygens. After ∼6 ps the H2 forms a bond with the central carbon and in a few ps a torsional rotation takes place, completing the transition to the global minimum. The activation barrier for the complete transition is around 50 kcal/mol (Table 1). Although this was a coarse exploration, an interesting pathway for this reaction, which samples all the relevant stationary points, was identified. Figure 8 shows a schematic energy profile of the trajectory for the reaction.

V. Conclusions

We have determined the optimized structures, relative energies and intramolecular reactions for two anions forms of malonic acid, anion malonate(−1) ($HO_2CCH_2CO_2^-$) and malonate(−2) ($^-O_2CCH_2CO_2^-$). A novel metadynamics method based on Car−Parrinello MD was used to help identify different minima and TS. The use of this method together with accurate quantum chemistry calculations allowed the identification of new malonate isomers (keto and enol structures), characterized by CO_2 rotations and intramolecular proton transfers. These proton transfers characterize the keto−enol tautomerism typical of these anions. In all cases, the keto tautomer is the more stable configuration. The metadynamics method allowed the system to explore the potential energy surface in a few picoseconds, crossing activation barriers of 20−50 kcal/mol. It revealed interesting pathways for conformational transitions and/or proton intramolecular transfer. In particular, the transition enol 1 → enol 2 → keto for the dianion was observed in a 10 ps run.

Acknowledgment. We thank Lee Pedersen for his many helpful suggestions. Support for this research was provided by NSF ITR-0121361 and CAREER-034039. We also thank NCSA for computer support.

References and Notes

(1) Francisco, J. S. *J. Chem. Phys.* **1992**, *96*, 1167.
(2) Iaonnoni, F.; Moule, D. C.; Clouthier, D. J. *J. Phys. Chem.* **1990**, *94*, 2290.
(3) Wiberg, K. B.; Laidig, K. E. *J. Am. Chem. Soc.* **1987**, *109*, 5935.
(4) Agranat, I.; Riggs, N. V.; Radom, L. *J. Chem. Soc., Chem. Commun.* **1991**, 80.
(5) Li, Y.; Houk, K. N. *J. Am. Chem. Soc.* **1989**, *111*, 4505.
(6) Nguyen, M. T.; Sengupta, D.; Raspoet, G.; Vanquickenbourne, L. G. *J. Phys. Chem.* **1995**, *99*, 11883.
(7) Gao, J.; Pavelites, J. J. *J. Am. Chem. Soc.* **1992**, *114*, 1912.
(8) Mavri, J.; Hodoscek, M.; Hadzi, D. *J. Mol. Struct.* **1990**, *209*, 421.
(9) Mauri, J.; Berendsen, J. C. *J. Phys. Chem.* **1995**, *99*, 12711.
(10) Simons, J.; Jordan, K. D. *Chem. Rev.* **1987**, *87*, 535.
(11) Scheller, M. K.; Compton, R. N.; Cederbaum, L. S. *Science* **1995**, *270*, 1160.
(12) Ding, C.-F.; Wang, X.-B.; Wang, L.-S. *J. Chem. Phys.* **1999**, *110*, 3635.
(13) Wang, L.-S.; Wang, X.-B. *J. Phys. Chem. A* **2000**, *104*, 1978.
(14) Aplin, R. T.; Moloney, M. G.; Newby, R.; Wright, E. J. *Mass Spectrom.* **1999**, *34*, 60.
(15) Roedern, E. G.; Grams, F.; Brandstetter, H.; Moroder, L. *J. Med. Chem.* **1998**, *41*, 339.
(16) Sadler, J. E. *Nature (London)* **2004**, *427*, 493.
(17) Gunawardena, N. R.; Brill, T. B. *J. Phys. Chem. A* **2001**, *105*, 1876.
(18) Merchán, M.; Tomás, F.; Nebot-Gil, I. *J. Mol. Struct. (THEOCHEM)* **1984**, *109*, 51.
(19) Bougeard, D.; Villepin, J. D.; Novak, A. *Spectrochim. Acta* **1988**, *44A*, 1281.
(20) Deerfield, D. W.; Pedersen, L. G. *J. Mol. Struct. (THEOCHEM)* **1996**, *368*, 163.
(21) Macoas, E. M. S.; Fausto, R.; Lundell, J.; Pettersson, M.; Khriachtchev, L.; Rasanen, M. *J. Phys. Chem. A* **2000**, *104*, 11725.
(22) Herbert, J. M.; Ortiz, J. V. *J. Phys. Chem. A* **2000**, *104*, 11786.
(23) Iannuzzi, M.; Laio, A.; Parrinello, M. *Phys. Rev. Lett.* **2003**, *90*, 238302-1.
(24) Laio, A.; Parrinello, M. *Proc. Natl. Acad. Sci. U.S.A.* **2002**, *99*, 12562.
(25) Car, R.; Parrinello, M. *Phys. Rev. Lett.* **1985**, *55*, 2471.
(26) Andersen, H. C. *J. Chem. Phys.* **1980**, *72*, 2384.
(27) Nose, S. *Mol. Phys.* **1984**, *52*, 255.
(28) *CPMD v3.9*; copyright IBM Corp. (1990−2004) and MPI fuer Festkoerperforschung, Stuttgart, Germany (1995−2001).
(29) Lee, C.; Yang, W.; Parr, R. *Phys. Rev. B* **1988**, *37*, 785.
(30) Handy, N. C.; Cohen, A. J. *Mol. Phys.* **2001**, *99*, 403.
(31) Laasonen, K.; Car, R.; Lee, C.; Vanderbilt, D. *Phys. Rev. B.* **1991**, *43*, 6796.
(32) Frisch, M. J.; et al. *Gaussian 03 (Revision B.01)*; Gaussian Inc.: Pittsburgh, PA, 2003.
(33) T. H. Dunning, J. *J. Chem. Phys.* **1989**, *90*, 1007.
(34) Becke, A. D. *Phys. Rev. A* **1988**, *38*, 3098.
(35) Onsager, L. *J. Am. Chem. Soc.* **1936**, *58*, 1486.
(36) Minofar, B.; Mucha, M.; Jungwirth, P.; Yang, X.; Fu, Y.-J.; Wang, X.; Wang, L. *J. Am. Chem. Soc.* **2004**, *126*, 11691.
(37) Gottschalk, K.; Hiskey, R.; Pedersen, L.; Koehler, K. *J. Mol. Struct. (THEOCHEM)* **1981**, *76*, 197.
(38) Han, S.; Kim, Y.; Kang, Y. *J. Mol. Struct. (THEOCHEM)* **1996**, *369*, 145.